Process Maps for Laser Deposition of Thin-Walled Structures

Aditad Vasinonta and Jack Beuth
Department of Mechanical Engineering
Carnegie Mellon University
Pittsburgh, PA

Michelle Griffith
Sandia National Laboratories
Albuquerque, NM

Abstract

In solid freeform fabrication (SFF) processes involving thermal deposition, thermal control of the process is critical for obtaining consistent deposition conditions and in limiting residual stress-induced warping of parts. In this research, nondimensionalized plots (termed process maps) are developed from numerical models of laser-based material deposition of thin-walled structures that map out the effects of changes in laser power, deposition speed and part preheating on process parameters. The principal application of this work is to the Laser Engineered Net Shaping (LENS) process under development at Sandia Laboratories; however, the approach taken is applicable to any solid freeform fabrication process involving a moving heat source. Similarly, although thin-walled structures are treated in the current work, the same approach could be applied to other commonly fabricated geometries. A process map for predicting and controlling melt pool size is presented and numerically determined results are compared against experimentally measured melt pool lengths for stainless steel deposition in the LENS process.

Nomenclature

T	= temperature	T_m	= melting temperature
T_{base}	= baseplate and wall preheat temperature	ρ	= density
k	= thermal conductivity	c	= specific heat
t	= wall thickness	h	= wall height
L	= wall length	l	= melt pool length
Q	= laser power	V	= travel speed of laser
α	= fraction of laser power absorbed by the wall		

Introduction

Residual stress-induced warping is a concern in nearly all solid freeform fabrication (SFF) processes. This includes processes based on successive curing of polymers as well as those based on successive thermal deposition of polymers or metals. In using SFF processes for rapid prototyping, some tolerance loss due to warping is generally acceptable; however, many targeted applications for using SFF processes as rapid manufacturing techniques (to create functional parts) have strict dimensional limits. For instance, injection molds typically consist of two or more parts that must fit precisely together. Residual stress-induced warping is also becoming a greater concern as SFF processes are used to build larger and larger parts, where larger part dimensions naturally lead to larger dimensional losses.

A critical issue in developing SFF processes as rapid manufacturing techniques is the alteration of the processes to control residual stresses while maintaining optimal deposition conditions. Because SFF processes are complicated, even an intuitive trial-and-error approach is unlikely to yield success in the near term. In this research, nondimensionalized plots (termed

process maps) are developed from numerical models of laser-based material deposition of thin-walled structures for this purpose. They map out the effects of changes in laser power, deposition speed and part preheating on process parameters. This paper specifically addresses control of melt pool size, which is critical for maintaining optimal deposition conditions.

The principal application of this work is to the Laser Engineered Net Shaping (LENS) process under development at Sandia National Laboratories [1]. In the LENS process, parts are constructed by focusing a high-power laser beam onto a metal substrate, where streams of metallic powder are simultaneously injected. The laser locally melts the powder to form a molten pool on the top surface of the growing part. By moving the laser beam, parts are built up, line by line and layer by layer. Work is underway at Sandia Labs to not only optimize process parameters manually, but to use real-time thermal images of melt pool size as a feedback mechanism controlling the process [2]. Process maps presented in this paper have been developed to aid in both manual and automated process control efforts. Although this research is directed toward the LENS process, the approach taken is applicable to any solid freeform fabrication process involving a moving heat source. Similarly, although thin-walled stainless steel structures are treated in the current work, the same approach could be applied to other commonly fabricated geometries and materials.

In the next section, the geometry analyzed is presented, along with details of the finite element model and boundary conditions used. A description of the analytical solution used to choose a nondimensionalization scheme for the results is also given. In the succeeding section, numerical results are presented in the form of a process map under the assumption of temperature-independent material properties. This version of the results is important to consider because within the assumption of temperature-independent properties it is applicable to any SFF process involving a moving heat source and for deposition of any single material. Temperature-dependent simulation results are then presented as applicable specifically to the deposition of stainless steel in the LENS process. Rules are given for how these results can be applied to the prediction and control of melt pool size, and results are also compared directly with measured melt pool lengths from the LENS process. Finally, process control-related insights apparent from the results are discussed.

Geometry Considered, Numerical Model and Analytical Solution

In the current study, the thin-walled structure shown in Fig. 1 is considered. Thin-walled geometries of this type are commonly fabricated using the LENS and other SFF processes. Also, numerical simulations of a wall of large height, h, with temperature-independent properties can be verified against an existing analytical solution in the literature.

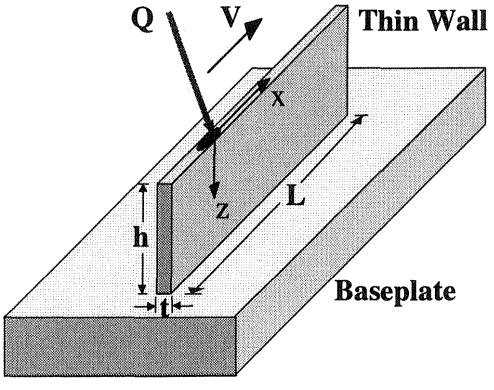

Figure 1. Thin-Walled Geometry Considered in This Study

The thin wall is assumed to be fabricated by depositing material along a single row; thus, the thickness of the wall is comparable to the molten melt pool size. The distance traveled by the laser and the length of the wall in the x direction are assumed large enough that steady-state conditions exist independent of the existence of the vertical free surfaces. It is assumed that the wall is built upon a large metallic substrate, which acts as a thermal heat sink and mechanically constrains the wall from deformation during the manufacturing process. Results presented herein demonstrate how melt pool length (extent in the x-direction) can be controlled as a function of wall height, h, absorbed laser power, αQ, laser velocity in the x direction, V, and uniform preheating of the wall and baseplate to a temperature $T = T_{base}$. Because results are presented as a function of absorbed laser power, it is presumed that the quantity α is well-defined.

The numerical models used in this study do not include effects of convective heat transfer from the wall free surfaces to the surrounding air and do not model convective flows in the melt pool itself. Work by Dobranich and Dykhuizen [3] suggests strongly that the role of these effects in determining melt pool size is not significant. The models of this study also model the laser as a point source of heat, neglecting the distribution of laser power over the melt pool region. Assuming a point source of power is reasonable given the goal of this study, which is to capture changes in melt pool size and other parameters as a function of changes in the process variables outlined above. Accuracy in the absolute predictions is of secondary importance. It is shown later in this paper, however, that model predictions still compare reasonably well with experimentally determined melt pool sizes.

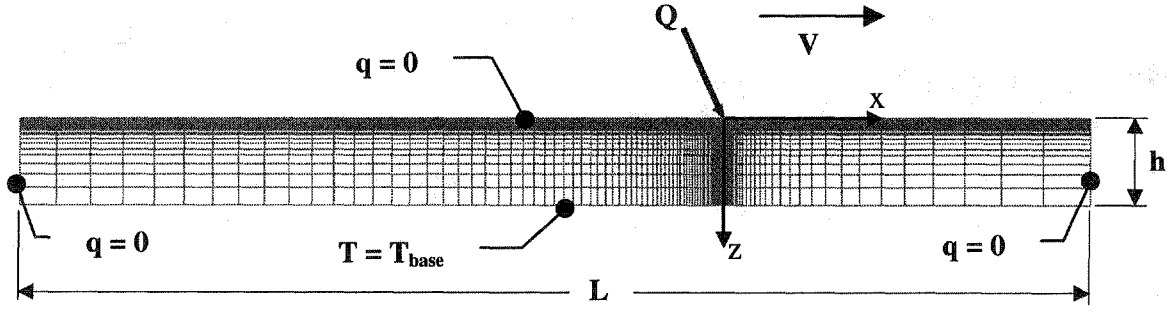

Figure 2. 2-D Thermal Model and Boundary Conditions

The mesh and boundary conditions used for a typical 2-D thermal model of this study are shown in Fig. 2. Four-noded bilinear thermal elements are used as part of the ABAQUS finite element software package. The laser beam focused on the top surface of substrate is simulated by a point source of power subsequently applied at model nodes at a rate simulating the laser velocity. Because of high temperature gradients in the region near heat source, the grid is biased toward the region that will surround the heat source at the time when results are to be extracted from the model. In addition to comparisons with an analytical solution valid for a large substrate, the convergence of this mesh was checked against a model with roughly half the resolution in the x and z directions with no noticeable change in the results.

As illustrated in Fig. 2, an insulated boundary condition is imposed on the top and both vertical sides of the substrate. The temperature along the substrate bottom is specified as fixed at a value equal to the temperature of the base plate. Sensitivity studies have shown that thermal results near the heat source are not significantly affected by boundary conditions along the substrate vertical and top surface being specified as either insulation or convective. Most of the heat transferred from the laser is conducted out through the bottom of the substrate. By using a 2-D model, it is also assumed that there is no heat loss through the front and back surfaces of the wall.

Thermal properties of AISI 304 stainless steel (SS304), which is used in the LENS and other SFF metal deposition processes, are used as inputs for the temperature-dependent simulations. Thermal properties were taken from [3] and are also comparable to those used by Klingbeil, et al. [4] in thermomechanical modeling of the Shape Deposition Manufacturing process. The properties used in the model that are set to depend on temperature are density, specific heat and thermal conductivity. The latent heat of the liquid-solid phase transition is also included in the model.

A 2-D conductive heat transfer solution for a point heat source moving across a semi-infinite thin substrate (Fig. 3) was first developed by Rosenthal [5]. The solution can be expressed in terms of modified Bessel function of second kind, zero order (K_0). An insightful study of application of this 2-D solution to the LENS process is given in [6] and [7].

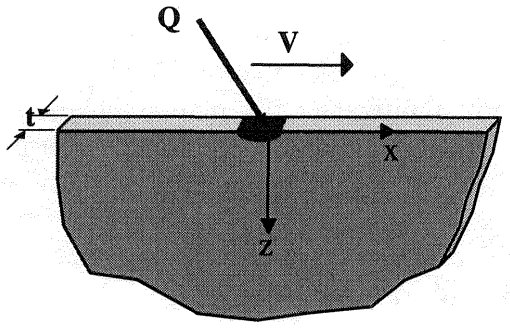

Figure 3. Geometry for the Analytical Model of Rosenthal [6]

The Rosenthal 2-D solution can be defined in terms of nondimensionalized variables as follows:

$$\bar{T} = e^{-\bar{X}_0} K_0\left(\sqrt{\bar{X}_0^2 + \bar{Z}_0^2}\right), \tag{1}$$

where

$$\bar{T} = \frac{T - T_{base}}{\alpha Q / \pi k t} \qquad \bar{X}_0 = \frac{x}{2k / \rho c V} \qquad \text{and} \qquad \bar{Z}_0 = \frac{z}{2k / \rho c V} \tag{2}$$

and where the origin of the coordinate axes is located at the (moving) point source location.

By using the above equations, the melt pool length on the top surface can be calculated if the (temperature-independent) material properties and process parameters, namely absorbed laser power, αQ, laser velocity, V, and base temperature, T_{base}, are known. As previously mentioned, the Rosenthal solution is for a 2-D semi-infinite substrate. The simulations of this study are designed to capture behavior for thin-walled structures having a finite height. To study the relation between the melt pool size and the height of the wall, two dimensionless length variables, the normalized melt pool length ($\bar{l}$) and normalized height of substrate ($\bar{h}$) are introduced as suggested by the Rosenthal solution:

$$\bar{l} = \frac{l}{2k / \rho c V} \qquad \text{and} \qquad \bar{h} = \frac{h}{2k / \rho c V}. \tag{3}$$

Similarly, a dimensionless melting temperature is introduced,

$$\bar{T}_m = \frac{T_m - T_{base}}{\alpha Q / \pi k t}, \tag{4}$$

so that results for normalized melt pool length, $\bar{l}$, are presented as a function of normalized wall height, $\bar{h}$, and normalized melting temperature, $\bar{T}_m$.

Results Assuming Temperature-Independent Properties

Assuming temperature-independent thermal properties, a process map for a thin-walled structure with a concentrated laser heat source moving across it can be developed directly, using the normalization scheme outlined in the previous section. The resulting process map is shown in Fig. 4, which consists of a surface plotted on 3 coordinate axes. This map was developed from several numerical simulations performed with differing wall heights in order to get the dependence of $\bar{l}$ on $\bar{h}$. The dependence of $\bar{l}$ on $\bar{T}_m$ was then determined from the same simulations by assuming different values of T_m.

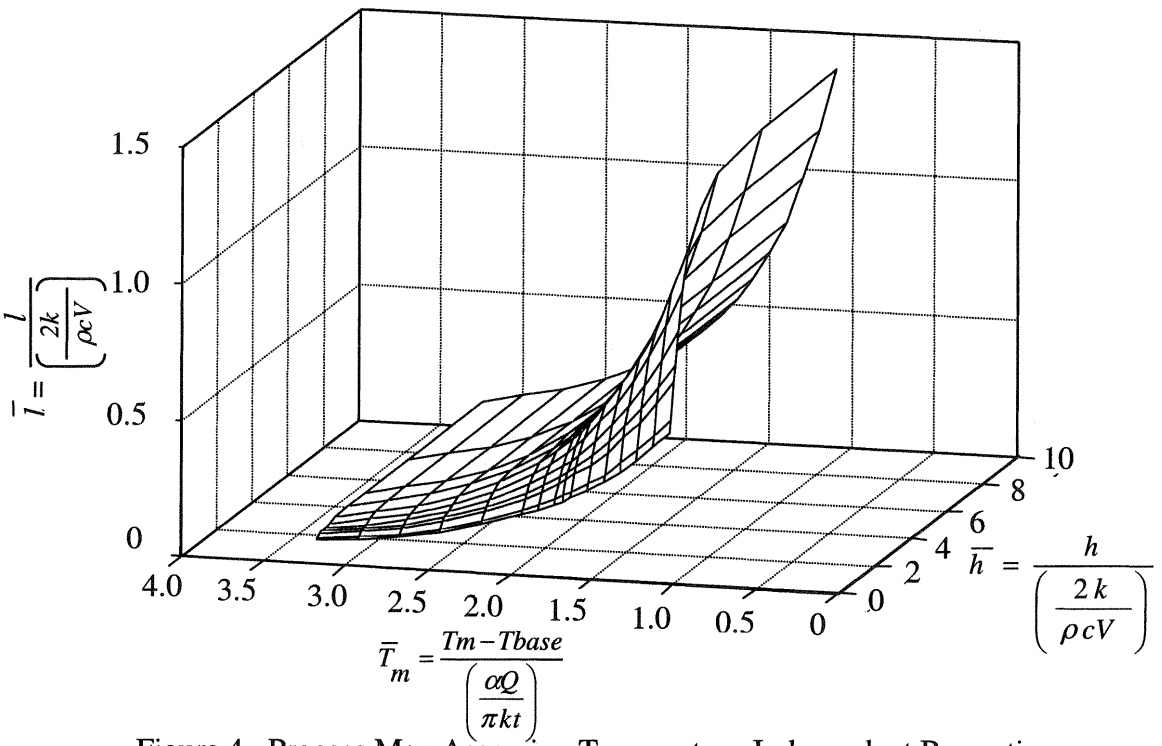

Figure 4. Process Map Assuming Temperature-Independent Properties

It can be seen from the plot that at each fixed $\bar{h}$, $\bar{l}$ increases with increasing T_{base} or Q (either of which decreases $\bar{T}_m$). Moreover, a change in T_{base} can be compensated for by a change in Q, to retain a desired melt pool length. When the wall is relatively tall, $\bar{h}$ has no significant effect on $\bar{l}$, because the wall is tall enough that the effect of the fixed temperature at the base is not felt at the melt pool. In contrast, $\bar{h}$ has a considerable effect on melt pool length when the wall is relatively short, with $\bar{l}$ dropping rapidly as $\bar{h}$ is reduced. It is recognized that the fixed temperature condition assumed for the 2-D model used herein will lose its validity for very small values of wall height. Thus the process map dependence on $\bar{h}$ is meant to only predict initial changes in melt pool size that can occur as wall height is reduced toward zero, or to predict the critical value of $\bar{h}$ when changes in melt pool size due to changes in wall height become significant. Melt pool size can also be increased through a decrease in laser velocity, V. This is most easily seen for large values of $\bar{h}$ (so that its dependence on V does not change $\bar{l}$). Through the normalization scheme used, the actual melt pool length, l, is given by:

$$l = 2k\bar{l} \Big/ \rho cV \cdot \tag{5}$$

Thus, for a fixed value of $\bar{l}$ as determined from the process map, l, is increased by a decrease in V.

It is important to emphasize that within the limitations of the assumption of temperature-independent properties, the process map shown in Fig. 4 is very general. It is applicable to any SFF process involving thermal deposition and for deposition of any single material and, as such, can be a useful intuitive guide to the control of SFF processes. However, for some material systems, if accurate predictions of the relationship between process variables and melt pool size are required, an accounting of the temperature dependence of thermal properties is needed.

Results for the LENS Process Using Temperature-Dependent Properties

In this section, results from modeling the LENS process for deposition of SS304 are presented, where temperature dependence of thermal properties is included in the modeling. The normalization scheme outlined in the previous section is still used, so that results are presented as a process map in terms of suitably normalized variables $\bar{T}_m$, $\bar{l}$ and $\bar{h}$. Because properties are temperature dependent, however, the map includes "error bars" that reflect the range in results seen when process variables are varied over the range of specific interest in the LENS process. That range consists of values of αQ from 43.2 to 165 W, V from 5.93 to 9.31 mm/sec and T_{base} from 30° C to 400° C.

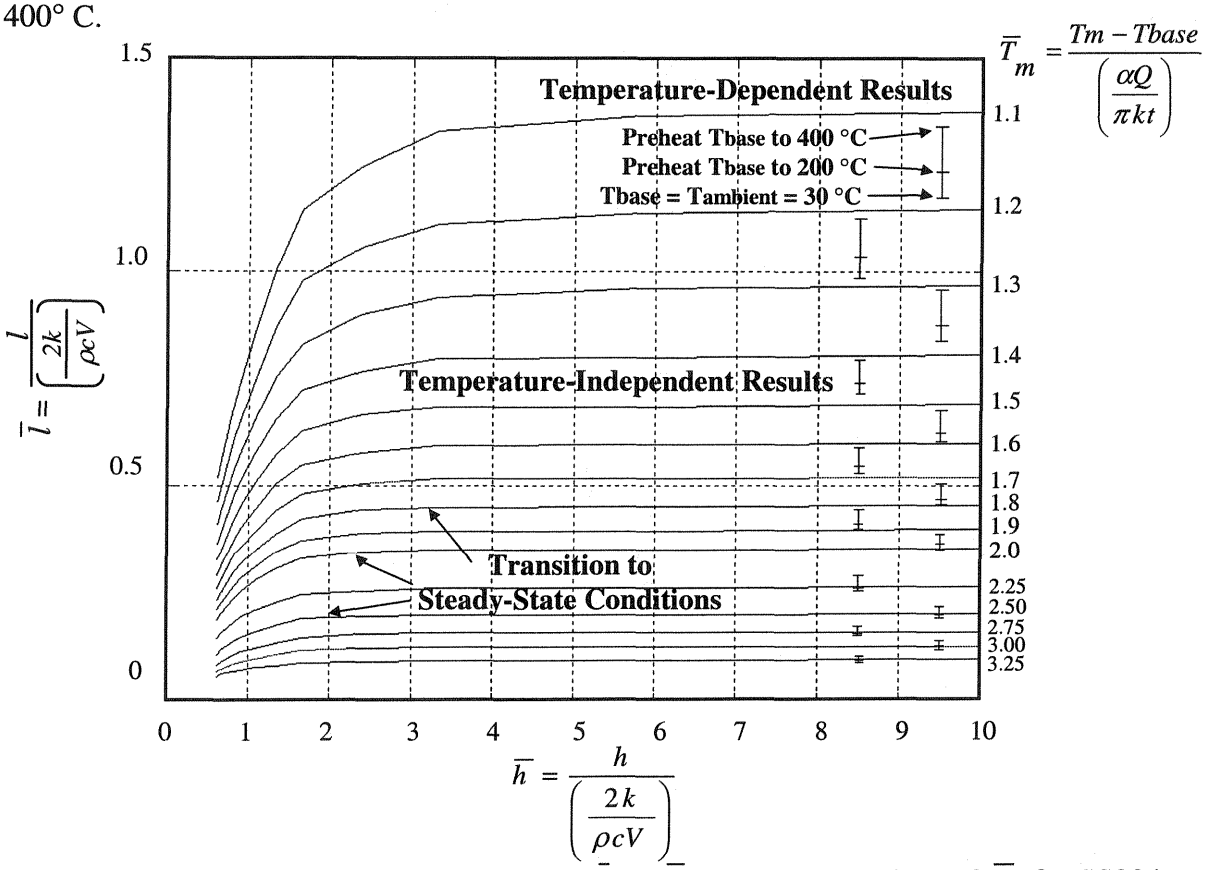

Figure 5. Temperature-Dependent Results of $\bar{l}$ vs. $\bar{h}$ for Various Values of $\bar{T}_m$ for SS304

Figure 5 gives a 2-D projection of the resulting map onto $\bar{l}$ vs. $\bar{h}$ axes for various values of $\bar{T}_m$. Lines in the plot are from temperature-independent simulations and the error bars in the region of large $\bar{h}$ values reflect results from temperature-dependent simulations. As indicated by the plot, the full range of results due to the temperature dependence of properties is less than 16% of the nominal value of $\bar{l}$. In order to obtain this level of agreement within the normalization scheme,

two rules were followed. First, all properties were normalized by the properties of SS304 at 1050K. This caused normalized temperature-dependent results as a function of laser power and velocity to nearly match normalized results from temperature-independent simulations for values of $\overline{T}_m$ from 1.60 to 3.25. Second, when including a preheat in the simulations, some accounting of the temperature dependence of material properties is required. As seen in the material properties in [3], the biggest percentage change in material properties with temperature is in thermal conductivity and the change is essentially linear in temperature. Thus when normalizing results in the presence of preheating, the conductivity is varied linearly with preheat temperature (in °C) by the relationship

$$k = 25.1 + 0.013(T_{base} - 30) \quad W/(mK). \qquad (6)$$

This linear change in conductivity with temperature has been chosen to best fit the results within the preheat range of 30° C to 400° C and is less per degree C than that of the k vs. T properties from [3]. In summary, the agreement seen in Figure 5 between temperature-independent and temperature-dependent results is accomplished by normalization by what could be considered an "effective" set of properties at 1050 K and a rudimentary accounting of temperature dependence of conductivity for cases including preheating.

A final issue that must be resolved in using the results of Fig. 5 is how to account for wall thickness. Wall thickness will also change with changes in process parameters and it has to be input into the 2-D model. Analysis of experimental results from Hofmeister and Wert [8] suggests strongly that wall thickness scales with melt pool length. Thus, in using the process map given in Fig. 5, the authors assume that wall thickness scales with melt pool size and that this scaling is unaffected by velocity (within the relatively narrow velocity range of 5.93 to 9.31 mm/sec). Because thickness is in the denominator of the dimensionless variable $\overline{T}_m$, accounting for thickness changes requires an iterative scheme, where the wall thickness, t, is changed until the ratio of t/l reaches its original value.

In summary, the process map of Fig. 5 can be used effectively for SS 304 deposition within the range of process parameters of interest in the LENS process by applying the following four rules:

1. Properties at 1050 K are used in the normalization;
2. For cases involving a change in preheat, a linear change in thermal conductivity with a preheat temperature is assumed, as given in eq. (6);
3. Wall thickness is assumed to scale with melt pool length; and
4. It is assumed that the melt pool length/wall thickness scaling is unaffected by velocity.

Figure 6 provides a comparison of measured melt pool lengths as a function of laser power and velocity to predictions provided by the process map of Fig. 5 using the rules outlined above. The only inputs used to generate the predictions from the process map were a single experimentally measured wall thickness for ambient conditions of V = 7.62 mm/sec and αQ = 100 W and an assumed value of α = 0.35 (as suggested by Dobranich and Dykhuizen [3]). Measurements were made using real-time thermal imaging methods described briefly in [2]. The experimental results presented are for a single set of observations [8] and do not reflect the variability seen in measured results at nominally identical conditions, which can easily be on the order of ± 5 %.

As seen in Fig. 6, for identical values of laser power and velocity, measured melt pool lengths are larger than predicted values. This is consistent with the model assumptions of a point source of heat and no convective flows in the melt pool, both of which tend to decrease melt pool length predictions. Clearly, however, the trends of melt pool length from both measurements and predictions are consistent for all three velocities.

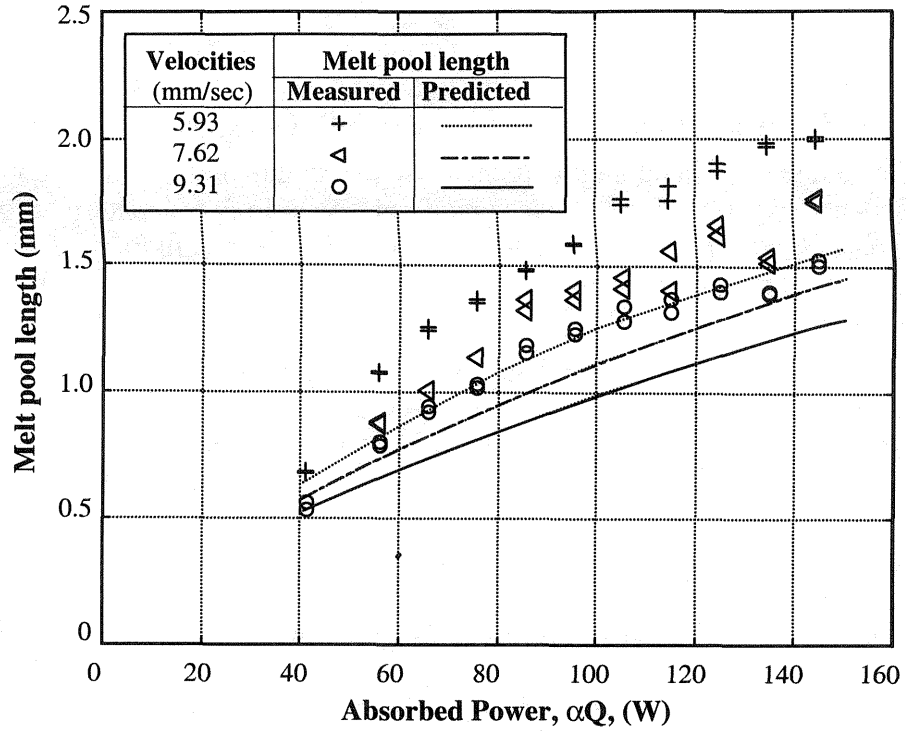

Figure 6. Predicted and Measured Melt Pool Lengths as a Function of Laser Power and Velocity

Summary and Implications of the Results

In this study, process maps have been developed for predicting or controlling melt pool size in the building of thin-walled structures by SFF processes. While the temperature-dependent results presented in this study are specifically applied to deposition of SS304 via the LENS process, temperature-independent results are applicable to any SFF process that involves a moving heat source. Furthermore, the approach taken here can be applied to other processes, materials and commonly encountered geometries. Analogous efforts are underway for developing process maps to control residual stress magnitudes primarily by part preheating. Such process maps could then be used with the process maps for melt pool length presented here to control residual stress magnitudes, while still maintaining an optimal melt pool length.

Although they are not presented in detail herein, calculations performed with the process maps described in this study have several major implications relevant to the LENS process and other similar SFF processes. First, results suggest that uniform preheating will not increase melt pool lengths significantly, and any increase in melt pool size can easily be eliminated by a small decrease in laser power or increase in laser velocity. Additionally, since uniform preheating will have an impact on residual stress magnitudes and warping, there is a clear possibility of using part preheating to reduce residual stresses with small changes in existing process parameters used to recover an optimal melt pool length. Second, a considerable change in melt pool length is predicted to occur for very short walls. It does not appear that this change can be compensated for by a base plate preheat alone. To obtain an optimal melt pool length for short walls, a change in laser power or laser velocity is needed.

Acknowledgements

This research has been supported by the National Science Foundation under grant DMI-9700320 and by Sandia National Laboratories under grant BE-0792. The authors would like to thank William Hofmeister and Melissa Wert of Vanderbilt University for providing data from their thermal imaging experiments that has proven to be vital for this research.

References

1. Griffith, M.L., Keicher, D.M., Atwood, C.L., Romero, J.A., Smugeresky, J.E., Harwell, L.D. and Greene, D.L., "Freeform Fabrication of Metallic Components Using Laser Engineered Net Shaping (LENS)," *Solid Freeform Fabrication Proceedings*, D.L. Bourell, J.J. Beaman, H.L. Marcus, R.H. Crawford and J.W. Barlow, eds., The University of Texas at Austin, August 1996, pp. 125-132.
2. Griffith, M.L., Schlienger, M.E. , Harwell, L.D., Oliver, M.S., Baldwin, M.D., Ensz, M.T., Smugeresky, J.E., Essien, M., Brooks, J., Robino, C.V., Hofmeister, W.H., Wert, M.J. and Nelson, D.V., "Understanding Thermal Behavior in the LENS Process," *Journal of Materials Design*, Vol. 20, No. 2/3, 1999, pp. 107-114.
3. Dobranich, D. and Dykhuizen, R.C., "Scoping Thermal Calculation of the LENS Process," Sandia National Laboratories Internal Report, 1998.
4 Klingbeil, N.W., Beuth, J.L., Chin, R.K. and Amon, C.H., "Measurement and Modeling of Residual Stress-Induced Warping in Direct Metal Deposition Processes," *Solid Freeform Fabrication Proceedings*, H.L. Marcus, J.J. Beaman, D.L. Bourell, J.W. Barlow, and R.H. Crawford, eds., The University of Texas at Austin, August 1998, pp. 367-374.
5. Rosenthal, D., "The Theory of Moving Sources of Heat and Its Application to Metal Treatments," *Transactions of ASME*, Vol. 68, 1946, pp. 849-866.
6. Dykhuizen, R.C. and Dobranich, D., "Cooling Rates in the LENS Process," Sandia National Laboratories Internal Report, 1998.
7. Dykhuizen, R.C. and Dobranich, D., "Analytical Thermal Models for the LENS Process," Sandia National Laboratories Internal Report, 1998.
8. Hofmeister, W.M. and Wert, M.J., personal communication.